

# Dynamics of Insulating Skyrmion under Temperature Gradient

Lingyao Kong<sup>1</sup> and Jiadong Zang<sup>1,2\*</sup>

<sup>1</sup> State Key Laboratory of Surface Physics and Department of Physics, Fudan University, Shanghai 200443, China

<sup>2</sup> Department of Physics and Astronomy, Johns Hopkins University, Baltimore, MD21218, U. S. A.

(Dated: March 15, 2018)

We study the Skyrmion dynamics in thin films under a temperature gradient. Our numerical simulations show that both a single and multiple Skyrmions in crystal move towards the high temperature region, which is the contrary to the particle diffusions. Noticing a similar effect in the domain wall motion, we employ a theory based on the magnon dynamics to explain this counter-intuitive phenomenon. Different from the temperature driven domain wall motion, Skyrmion's topological charge plays an important role, and a transverse Skyrmion motion is observed. Our theory turns out to be in agreement with the numerical simulations, both qualitatively and quantitatively. Our calculation indicates a very promising Skyrmion dynamic phenomenon to be observed in experiments.

PACS numbers: 75.70.Kw, 75.10.Hk, 66.30.Lw, 75.40.Mg

A Skyrmion is a topological configuration in which local spins wrap around the unit sphere for an integer number of times[1]. After decades of theoretical discussions[2, 3], it has been recently observed in the bulk sample of MnSi[4]. This material is a typical helimagnet where inversion asymmetry induced Dzyaloshinsky-Moriya (DM) interaction is significant; the latter plays an important role to generate Skyrmion configurations. Their neutron scattering study shows that Skyrmions perfectly pack themselves in triangle crystals as a compromise between DM interaction and ferromagnetic Heisenberg exchange. However, due to the competition between conical phase, the Skyrmion phase unfortunately survives only in a narrow window at finite temperatures[4]. Later, real space image in Fe<sub>x</sub>Co<sub>1-x</sub>Si thin film[5] has demonstrated that a Skyrmion crystal phase can be considerably enlarged in two dimensions, and stable down to zero temperature [6–8]. Further exploration shows that Skyrmion phases are not only present in these two metallic materials, but also in insulating materials like Cu<sub>2</sub>OSeO<sub>3</sub>[9] and BaFe<sub>1-x-0.05Sc<sub>x</sub>Mg<sub>0.05</sub>O<sub>19</sub>[10].</sub>

After the discovery of Skyrmion crystals, numerous efforts has been devoted to the manipulations of Skyrmions. Due to their topological nature, Skyrmions remain stable against moderate perturbations. Therefore, controlling the motion of Skyrmions would allow for potential applications of Skyrmion physics. To this end, Skyrmion dynamics has been discussed in detail[11–13]. One well accepted way to control the motion of Skyrmions in metallic thin films is via a current. Unlike the regular domain wall motion driven by the current, the Skyrmion motion can occur at a tiny current threshold[14]. This advantage makes low-dissipative Skyrmion manipulation possible. An interesting question is if it is possible to drive the motion of insulating Skyrmions. If the answer is positive, one can thoroughly get rid of the dissipations from the conducting current.

In this letter, we study the directional motion of insulating Skyrmions under a temperature gradient. Insulating materials help us to get rid of the influence from conduction electrons[14, 15]. Interestingly, our study shows that Skyrmions unconventionally move towards high temperature regions, contrary to the usual Brownian motion. A Skyrmion as a large-size quasi-particle appears to have negative diffusive coefficient. Followed by numerical simulations, a magnon assisted theory is employed to explain this novel phenomenon.

*Numerical Simulation:* To simulate the magnetization dynamics at finite temperature, the stochastic Landau-Lifshitz-Gilbert (LLG) approach is employed[16, 17]. The effect of the thermal fluctuation at the temperature  $T$  is characterized by a random field  $\mathbf{L}$  in addition to the usual LLG equation. The equation of motion is given by

$$\dot{\mathbf{m}} = -\gamma \mathbf{m} \times (\mathbf{H}_{eff} + \mathbf{L}) + \alpha \mathbf{m} \times \dot{\mathbf{m}} \quad (1)$$

where  $\gamma = g/\hbar$  is the gyromagnetic ratio and  $\alpha$  is the Gilbert damping coefficient. The magnitude of the magnetization  $\mathbf{m}$  is normalized to unity. In the case of ferromagnetic insulators,  $\alpha$  can be tiny, due to the absence of conduction electrons to dissipate the magnetization energy.  $\mathbf{H}_{eff} = -\partial H/\partial \mathbf{m}$  is the effective field acting on the local magnetization  $\mathbf{m}$ . In order to eventually achieve thermal equilibrium eventually, the dissipation-fluctuation relation  $\langle L_\mu(\mathbf{r}, t) L_\nu(\mathbf{r}', t') \rangle = \xi \delta_{\mu\nu} \delta(\mathbf{r} - \mathbf{r}') \delta(t - t')$  is satisfied, where  $\xi = \alpha a^2 k_B T / \gamma$  and  $a$  is the lattice constant. The average  $\langle \rangle$  is taken over all the realizations of the fluctuation field. Here, a uniform but small temperature gradient is assumed. As the thermal fluctuation of each spin is about  $k_B T$ , which is about  $J/10$  in our simulation. As long as it is larger than the temperature difference between neighboring sites, the local equilibrium can be established and this stochastic LLG approach is justified. In this case,  $\xi$ , together with  $T$ , is a linear function of the position. In what follows, the temperature gradient is turned on longitudinally along the  $x$  direction. Numerically, the stochastic field  $L_\mu(\mathbf{r}, t)$  is created by a random number generator with the mean square controlled by the temperature, and the stochas-

\*Electronic address: jiadongzang@gmail.com

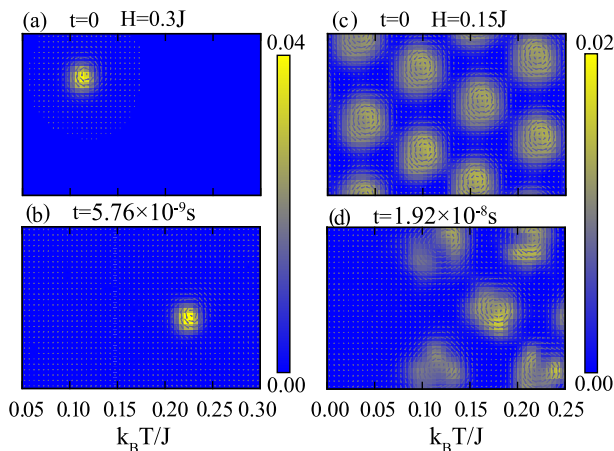


FIG. 1: Snapshots of Skymion motions. Color bars stand for the topological charge density  $q$ . At the critical magnetic field of  $H = 0.3J$ , single Skymion is generated (a). Under temperature gradient, it moves from low to high temperature (b). Skymion crystal moves in a similar way under a lower magnetic field  $H = 0.15J$  (c, d).

tic LLG equation Eq.(1) is integrated out in the deterministic Heun scheme[16], with a time step of  $0.05\hbar/J$ . The initial Skymion configurations are given by classical Monte Carlo updates followed by further relaxation realized by solving the LLG equation with a fourth order Runge-Kutta method[5].

We employed the standard model given by

$$H = \sum_{\langle ij \rangle} [-J\mathbf{m}_i \cdot \mathbf{m}_j + \mathbf{D}_{ij} \cdot (\mathbf{m}_i \times \mathbf{m}_j)] - \sum_i \mathbf{H} \cdot \mathbf{m}_i \quad (2)$$

where the DM vector  $\mathbf{D}_{ij} = D\hat{\mathbf{r}}_{ij}$  points from one local magnetization to the other. The magnetic field  $\mathbf{H} = H\hat{z}$  is perpendicular to the film.  $H$  relates the real magnetic field  $h$  by  $H = \mu_B h$ . In the simulations, the Heisenberg exchange  $J/k_B = 50K$ , and the strength of DM interaction  $D = 0.5J$ . Note in reality,  $D$  is an order of magnitude smaller. The advantage of large  $D$  in current simulation is to reduce the Skymion radius and save the calculation resources. The lattice spacing  $a$  is  $5\text{\AA}$ , and the full simulated sample size is  $150a \times 50a$ , which is much larger than the Skymion radius (about  $5a$ ). Therefore the finite size effect is safely negligible. Gilbert damping  $\alpha$  is set to be 0.1. This value is relatively larger than the realistic case, but it is helpful to get a relatively larger stochastic field to make the Skymion motions transparent in simulations.

The phase diagram of the Hamiltonian in Eq.(2) is already known[5, 18]. The phase transition between the Skymion crystal and the ferromagnetic phase appears to be of first order and, therefore, the coexistence of both phases are observed. By tuning the external magnetic field  $H$  up to a critical value, the Skymion crystal is melted so that one can have chance to get a single Skymion on the thin film. The snapshots of a single Skymion are shown in Fig.1(a). Once the mag-

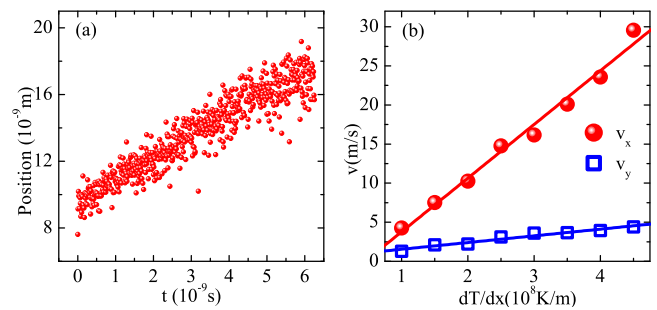


FIG. 2: (Color online.) (a) A typical simulation showing the Skymion's instant longitudinal positions. Although it fluctuates at under finite temperature, a forward average velocity is observed. (b) A linear scaling between the longitudinal velocity and the temperature gradient (red line). A nonvanishing  $v_y$  also addressed (blue line), indicating the Skymion Hall effect.

netic field is further reduced, a perfect Skymion crystal is energetically favored (Fig.1(c)). The color bars in these plots indicate the topological charge density  $q = \frac{1}{4\pi} \mathbf{m} \cdot (\partial_x \mathbf{m} \times \partial_y \mathbf{m})$ . The total topological charge  $Q = \int d^2\mathbf{r}q$  counts the number of Skymions in the lattice.

As the simulation goes on, the single Skymion starts to move under the effect of the stochastic field. Although the instant velocity appears to be random, the overall velocity is nonzero. Quantitatively, we can define the center position  $\mathbf{r}_c$  of the Skymion weighed by the topological charge:  $\mathbf{r}_c = \int d^2\mathbf{r} \mathbf{m} \cdot (\partial_x \mathbf{m} \times \partial_y \mathbf{m}) \mathbf{r} / \int d^2\mathbf{r} \mathbf{m} \cdot (\partial_x \mathbf{m} \times \partial_y \mathbf{m})$ . Fig.2(a) shows a typical simulation result of the relation between the center position and the simulation time. At short time scales, the Skymion oscillates around an average position, in accordance with the thermal fluctuation. In the long run, the Skymion drifts directionally. The mean velocity is derived by averaging over 1000 simulated events. Its relation with the temperature gradient is shown in Fig.2(b). The longitudinal velocity is proportional to the temperature gradient. Meanwhile, the transverse velocity is nonzero and linear in temperature gradient as well, although the magnitude is one order of magnitude smaller than the longitudinal one. The transverse motion of Skymion is another example of the Skymion Hall effect in analogy to the conventional Hall effect for electrons[11].

A surprising result is that the Skymion moves from the low temperature region to the high temperature one, as shown in Fig.1(b). It is generally known that under a temperature gradient, particles like electrons should move to the cold terminal, due to the low density of hot particles at the cold end. This directional Brownian motion gives rise to various phenomena such as the Seebeck effect. Our result contradicts this physical picture. This effect even holds also for the entire Skymion crystal in which multiple Skymions are driven by the temperature gradient. As shown in Fig.1(d), the whole crystal shifts towards high temperatures in a similar way. However,

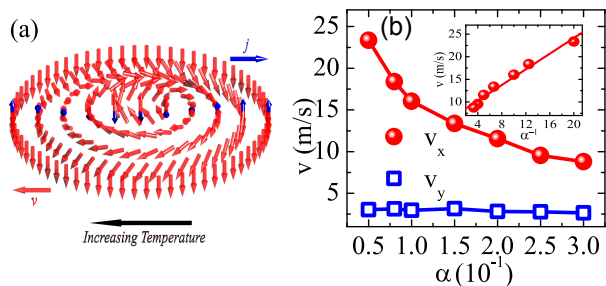


FIG. 3: (Color online.) (a) Sketch of physical picture for the Skymion motion towards high temperature. Red arrow stands for the local magnetization constructing the Skymion configuration. Blue arrow stands for the spin of magnon, which points opposite to the local magnetization. Under a temperature gradient, magnons move from the high temperature region to the low temperature one indicated by  $j$ , resulting in an opposite motion  $v$  for the Skymion. (b) The scaling of Skymion velocity with the Gilbert damping  $\alpha$ .  $v_x$  is inversely proportional to  $\alpha$  (red line and the inset).  $v_y$  is almost independent of  $\alpha$  (blue line).

the crystal melts a little bit during the diffusion process.

*Theory:* In order to understand the counter-intuitive diffusion direction, a magnon assisted theory is employed[19]. In the simplest case of a ferromagnet polarized along  $\hat{z}$ , the spin's deviation  $(n_x, n_y)$  from its equilibrium direction is described by the presence of magnons. The magnon creation operator is  $a^\dagger = (n_x - in_y)/\sqrt{2}$ , and the magnon number operator is  $\rho = a^\dagger a = \frac{1}{2}(n_x^2 + n_y^2)$ . The spin component along the equilibrium direction is simply  $n_z = \sqrt{1 - (n_x^2 + n_y^2)} \approx 1 - \rho$ . This result shows that each magnon carries spin one polarized antiparallely with the equilibrium direction. Therefore, once there is a Skymion under a temperature gradient, as shown in Fig.3(a), magnon as a low-lying excitation responds much more actively than the Skymion itself. As a typical quasiparticle, the magnon diffuses from hot to cold end in the usual way. Due to the antiparallel alignment of the spin, the magnon current provides a negative transfer torque on the Skymion. Due to the conservation of the total angular momentum, the Skymion moves in the opposite way.

To quantitatively formulate this physical picture, let's decompose the local magnetizations into the slow mode  $\mathbf{m}_s$  and the orthogonally fast mode  $\mathbf{m}_f = \mathbf{m}_s \times \mathbf{n}$ :  $\mathbf{m} = (1 - \mathbf{m}_f^2)^{1/2} \mathbf{m}_s + \mathbf{m}_f$ . The slow mode is responsible for the equilibrium configuration of the Skymion. Substituting it into the continuum version of the Hamiltonian  $H = \int d^2r [\frac{1}{2}J(\nabla \mathbf{m})^2 + \frac{D}{a} \mathbf{m} \cdot (\nabla \times \mathbf{m}) - \frac{\mathbf{H}}{a^2} \cdot \mathbf{m}]$  and keeping only the dominant terms arising from the fluctuations of fast mode, one can get the following equation of motion for the slow mode[18, 19]:

$$\dot{\mathbf{m}}_s = -\gamma J a^2 \mathbf{j} \cdot \nabla \mathbf{m}_s - \gamma \mathbf{m}_s \times \mathbf{L} + \alpha \mathbf{m}_s \times \dot{\mathbf{m}}_s \quad (3)$$

where  $j_i = \mathbf{m}_s \cdot (\mathbf{n} \times \partial_i \mathbf{n}) = i(\partial_i a^\dagger a - a^\dagger \partial_i a)$  is the magnon current induced by the temperature gradient. Note that

the first term on the right hand side of Eq.(3) is analogous to the spin transfer torque provided by the itinerant electrons in the adiabatic limit[11, 20]. However the sign is different in the two cases. The negative sign here corresponds to the negative transfer torque from the magnons.

Ignoring the deformation of the Skymion, the slow modes can be written in terms of the collective coordinates  $\mathbf{u}(t)$  as  $\mathbf{m}_s(r, t) = \mathbf{m}_s^0(\mathbf{r} - \mathbf{u}(t))$ , where  $\mathbf{m}_s^0$  is the ground configuration, and  $\mathbf{u}(t)$  describes the position of the Skymion. Inserting it into Eq.(3) and integrating over the ground configuration, one finally gets the equation motion for the collective coordinates  $Q \varepsilon^{ij} \dot{u}_j(t) = Q \gamma J a^2 \varepsilon^{ij} j_j + 2\alpha \eta \dot{u}_i(t) + \frac{\gamma}{4\pi} \int d^2r \partial_i \mathbf{m}_s^0 \cdot \mathbf{L}(\mathbf{r} + \mathbf{u}, t)$ , where the shape factor  $\eta = \frac{1}{8\pi} \int d^2r \partial_i \mathbf{m}_s^0 \times \partial_i \mathbf{m}_s^0$  is close to unity. We define a collective stochastic force  $l_i$  acting on the Skymion as a whole by  $l_i(\mathbf{u}, t) = \int d^2r \partial_i \mathbf{m}_s^0 \cdot \mathbf{L}(\mathbf{r} + \mathbf{u}, t)$ , whose average then satisfies  $\langle l_i(\mathbf{u}, t) l_j(\mathbf{u}', t') \rangle = \xi' \delta_{ij} \delta(\mathbf{u} - \mathbf{u}') \delta(t - t')$  with a new mean square  $\xi' = 8\pi \eta \xi = 8\pi \alpha \eta a^2 k_B T / \gamma$ . The collective equation of motion resembles the standard Langevin equation. Let  $P(\mathbf{r}, t)$  be the probability to find the Skymion at position  $\mathbf{r}$  and the time  $t$ . It thus satisfies the Fokker-Planck equation[21]:  $\frac{\partial P}{\partial t} = -[\gamma J a^2 j_x - 2(\frac{\gamma}{4\pi Q})^2 (\partial_x \xi')^2] \partial_x P - \gamma J a^2 j_x \cdot 2\alpha \eta \partial_y P + (\frac{\gamma}{4\pi Q})^2 \xi' (\partial_x^2 + \partial_y^2) P$ . At the current stage, we are only interested in the lowest order traveling wave solution of the Fokker-Planck equation, namely  $P(\mathbf{r}, t) = P(\mathbf{r} - \mathbf{v}t)$ . The last term provides nonlinearity: it thus broadens the wave package and can be neglected. Finally, we get the average velocity of the Skymion in both the longitudinal and transverse directions

$$v_x = \gamma J a^2 j_x - \frac{\gamma}{\pi Q^2} \alpha \eta a^2 k_B \frac{dT}{dx} \equiv v_x^M - v^B \quad (4)$$

$$v_y = 2\alpha \eta v_x^M \quad (5)$$

The contributions from the magnon and the Brownian motion are separable and are denoted, respectively, by  $v_{x,y}^M$  and  $v^B$ . Eq.(4) shows explicitly that their effects are completely opposite: the Skymion is pushed by the Brownian motion towards the cold terminal, while it is pulled back to the hot end by the magnon. On the other hand, as the temperature gradient is exerted along the  $x$  direction, the Brownian motion along the  $y$  direction vanishes on the average. Only the magnon effect contributes to the transverse velocity, which is a factor  $\alpha$  smaller than the longitudinal one, agreeing with the numerical simulation in Fig.2b. This Hall effect of the Skymion motion is closely related to the topology of the Skymion texture captured by the nonzero topological charge  $Q$ . Generally speaking, a directional transverse motion requires the breaking of time reversal symmetry. Here it is the dissipative damping  $\alpha$  that breaks time reversal. Therefore one expects the proportionality between transverse velocity and Gilbert damping  $\alpha$ .

Now it is important to evaluate the magnon current. To this end, we can apply a semi-classical approach with the relaxation time approximation[22]. The variation from the Bose-Einstein distribution  $f$  is given by

$\delta f = \tau \frac{\partial f}{\partial \varepsilon} \frac{\varepsilon}{T} \mathbf{v} \cdot \nabla T$ .  $\tau$  is the relaxation time. The magnon current is consequently  $j = a^2 \int \frac{d^2 k}{(2\pi)^2} k_x a_k^\dagger a_k = a^2 \int \frac{d^2 k}{(2\pi)^2} \tau k_x \frac{\partial f}{\partial \varepsilon} \frac{\varepsilon}{T} \frac{\partial \varepsilon}{\hbar \partial k_x} \frac{dT}{dx}$ . In this simple evaluation, higher order processes such as magnon-magnon interactions are neglected so that  $\tau$  is given by the Gilbert damping only. In the presence of a nonzero  $\alpha$ , the magnon frequency acquires an imaginary value  $\alpha\omega$ . Therefore the magnon number decays exponentially as  $\rho(t) \sim \exp(-2\alpha\omega t)$ . The relaxation time is thus  $\tau = 1/(2\alpha\omega)$ . According to the work by Petrova and Tchernyshyov[23], linear dispersion is respected in the Skyrmion crystal, given by  $\varepsilon\hbar\omega = \frac{1}{2}M_0 D \alpha \gamma \hbar k \equiv s\hbar k$ , where  $M_0$  is the magnitude of the local spin.  $s$  is the effective velocity of the magnon. Finally one gets the magnon current given by

$$j = j_x = \frac{\pi}{24} a^2 \left(\frac{k_B}{\hbar s}\right)^2 \frac{T}{\alpha} \frac{dT}{dx} \quad (6)$$

This result indicates that the magnon current, as well as the Skyrmion velocity, is proportional to the temperature gradient. It is quite consistent with the numerical result in Fig.2. This evaluation also explains the reason why the magnon contribution is overwhelming in Eq.(4). The ratio between these two contributions is  $v^B/v_x^M = \frac{6}{\pi} \alpha^2 \frac{D^2}{J k_B T}$ . It is definitely a small number due to the small DM interaction and the tiny damping coefficient. The net effect of the Brownian motion is almost invisible in this case.

Another interesting conclusion from Eq.(6) is that  $j$  is inversely proportional to  $\alpha$ . Consequently, the longitudinal Skyrmion velocity is also inversely proportional to  $\alpha$ , while the transverse velocity is independent of  $\alpha$ . In reality, dislocations or imperfections of the Skyrmion lattice may affect the magnon dispersion significantly. However, as long as the magnon-magnon interaction is negligible, the inverse proportionality between the longitudinal velocity and the Gilbert damping always holds. In the case of insulating helimagnets, as the magnetization energy can hardly be dissipated away, the Gilbert damping is tiny. The Skyrmion velocity can be quite large instead. In order to test this theory, we scaled the velocity with respect to  $\alpha$  from the simulations, as shown in Fig.3(b). A nice inverse proportionality between  $v_x$  and  $\alpha$  is explicitly addressed.  $v_y$  remains almost the same for different  $\alpha$  values. These results match well with our theory.

A similar magnon assisted theory was applied to the case of domain wall motion[17, 19]. However, the difference brought by the topology of the Skyrmion is profound. In the derivation of collective equation of motion, the quantization of topological charge  $Q$  is applied, which is the key feature of the Skyrmion. For the domain wall case, the total topological charge vanishes, so that

this method doesn't apply. The collective equation of motion for the Skyrmion provides us a universal dynamics that weakly depends on the detailed structure of the Skyrmion. Furthermore, the Skyrmion stability allows us to treat it as a quasiparticle, so that the Fokker-Planck equation comes into play. The generalization from 1D domain wall to 2D Skyrmion crystal brings new phenomena such as the Skyrmion Hall effect.

*Estimates:* For  $\text{Cu}_2\text{OSeO}_3$ ,  $J/k_B \sim 50\text{K}$ ,  $M_0 = 1/2$ , and the spiral period is  $\lambda \approx 2\pi J a/D \sim 50\text{nm}$ [9]. Let  $a \sim 5\text{\AA}$ , thus  $D/k_B \sim 3\text{K}$ , and the effective velocity  $s \sim 15.6\text{m/s}$ . As a reasonable estimate, let  $\alpha = 0.01$ , then our theory gives  $v_x \sim 1.2 \times 10^{-4} \frac{dT}{dx} (\text{m/s})$ . In the numerical simulations,  $v_x \sim 10^{-7} \frac{dT}{dx}$  for  $\alpha = 0.1$ . This three orders of magnitude of difference can be perfectly fixed by noting a difference of a factor  $\sim 10$  in DM interaction  $D$ , and another factor 10 in the Gilbert damping  $\alpha$ . This serves as a quantitative confirmation of our theory. Experimentally a reasonably large temperature gradient is about 1K per millimeter[24], so that a velocity of 0.1m/s can be achieved. This Skyrmion motion can be traced by real-space spectroscopies such as the Lorentz TEM. Another interesting issue is how to observe this phenomenon by transport measurements. As itinerant electrons are absent, signals of the topological Hall effect present in metallic Skyrmion crystals[25, 26] is missing here. Probably the measurement technique of the spin Seebeck effect would come to help as a moving Skyrmion carries a spin current. There's no spin polarized electron current in this system, so that the signal of the moving Skyrmion would be dominant.

Compared to the domain wall motion, a peculiar advantage of the Skyrmion motion is its tiny pinning indicated by the small threshold current in current driven case. This pinning results from impurities and lattice imperfections, which have basically the same level in insulating and metallic Skyrmion crystals. A low critical current of  $10^6\text{A/m}^2$  is observed in MnSi[14], which corresponds to a theoretical velocity of  $10^{-4}\text{m/s}$ [11]. Our estimate of the temperature gradient driven Skyrmion motion is far beyond this threshold, thus it can be easily realized. The interaction between magnon and Skyrmion discussed here might open a new field of 'Skyrmionic magnonics'.

We are grateful for the insightful discussions with A. Abanov, Cosimo Bambi, S. X. Huang, N. Nagaosa, V. Vakaryuk, O. Tchernyshyov, Y. Tserkovnyak, and Hui Wang. This work was supported in part by the Theoretical Interdisciplinary Physics and Astrophysics Center and by the U.S. Department of Energy, Office of Basic Energy Sciences, Division of Materials Sciences and Engineering under Award DEFG02-08ER46544, and Fudan Research Program on Postgraduates.

[1] T. H. R. Skyrme, Proc. Roy. Soc. London A **260**, 127 (1961); Nuc. Phys. **31**, 556 (1962).

[2] A.N. Bogdanov and D. A. Yablonskii, Sov. Phys. JETP

- 68, 101-103 (1989)
- [3] U.K. Rößler, A.N. Bogdanov, and C. Pfleiderer, *Nature* **442**, 797-801 (2006).
- [4] S. Mühlbauer, B. Binz, F. Jonietz, C. Pfleiderer, A. Rosch, A. Neubauer, R. Georgii, and P. Böni, *Science* **323**, 915 (2009).
- [5] X. Z. Yu *et al.*, *Nature (London)* **465**, 901 (2010).
- [6] S. D. Yi, S. Onoda, N. Nagaosa, and J. H. Han, *Phys. Rev. B* **80**, 054416 (2009).
- [7] U. K. Rößler, A. A. Leonov, and A. N. Bogdanov, arXiv:1009.4849.
- [8] J. H. Han, J. Zang, Z. Yang, J. H. Park, and N. Nagaosa, *Phys. Rev. B* **82**, 094429 (2010).
- [9] S. Seki, X. Z. Yu, S. Ishiwata, and Y. Tokura, *Science*, **336**, 198 (2012).
- [10] X. Z. Yu *et al.*, *PNAS* **109**, 8856 (2012).
- [11] J. Zang, M. Mostovoy, J. H. Han, and N. Nagaosa, *Phys. Rev. Lett.* **107**, 136804 (2011).
- [12] T. Schulz *et al.*, *Nat. Phys.* **8**, 301 (2012).
- [13] M. Mochizuki, *Phys. Rev. Lett.* **108**, 017601 (2012).
- [14] F. Jonietz *et al.*, *Science* **330**, 1648 (2010).
- [15] K. Everschor, M. Garst, B. Binz, F. Jonietz, S. Mühlbauer, C. Pfleiderer, and A. Rosch, *Phys. Rev. B* **86**, 054432 (2012).
- [16] J. L. García-Palacios, and F. J. Lázaro, *Phys. Rev. B* **58**, 14937 (1998).
- [17] D. Hinzke and U. Nowak, *Phys. Rev. Lett.* **107**, 027205 (2011).
- [18] See supplemental material.
- [19] A. A. Kovalev, and Y. Tserkovnyak, *Europhys. Lett.* **97**, 67002 (2012).
- [20] G. Tatara, H. Kohno, and J. Shibata, *Phys. Rep.* **468**, 213 (2008).
- [21] H. Risken, *The Fokker-Planck Equation*, 2nd ed. (Springer, Berlin, 1989).
- [22] N. W. Ashcroft, and N. D. Mermin, *Solid State Physics*, Saunders College 1976.
- [23] O. Petrova, and O. Tchernyshyov, *Phys. Rev. B* **84**, 214433 (2011).
- [24] K. Uchida, S. Takahashi, K. Harii, J. Ieda, W. Koshibae, K. Ando, S. Maekawa and E. Saitoh, *Nature* **45**, 778 (2008).
- [25] A. Neubauer *et al.*, *Phys. Rev. Lett.* **102**, 186602 (2009).
- [26] S. X. Huang, and C. L. Chien, *Phys. Rev. Lett.* **108**, 267201 (2012).

## I. NUMERICAL DETAILS

The lattice Hamiltonian in the numerical simulations is given by

$$\begin{aligned}
 H = & -J \sum_{\mathbf{r}} \mathbf{m}_{\mathbf{r}} \cdot (\mathbf{m}_{\mathbf{r}+\hat{x}} + \mathbf{m}_{\mathbf{r}+\hat{y}}) \\
 & -D \sum_{\mathbf{r}} [\hat{x} \cdot (\mathbf{m}_{\mathbf{r}} \times \mathbf{m}_{\mathbf{r}+\hat{x}}) + \hat{y} \cdot (\mathbf{m}_{\mathbf{r}} \times \mathbf{m}_{\mathbf{r}+\hat{y}})] \\
 & -H \sum_{\mathbf{r}} m_{\mathbf{r}}^z
 \end{aligned} \tag{7}$$

where the first term is the ferromagnetic Heisenberg exchange, the second term is the Dzyaloshinskii-Moriya interaction, and the last term is the Zeeman coupling. The

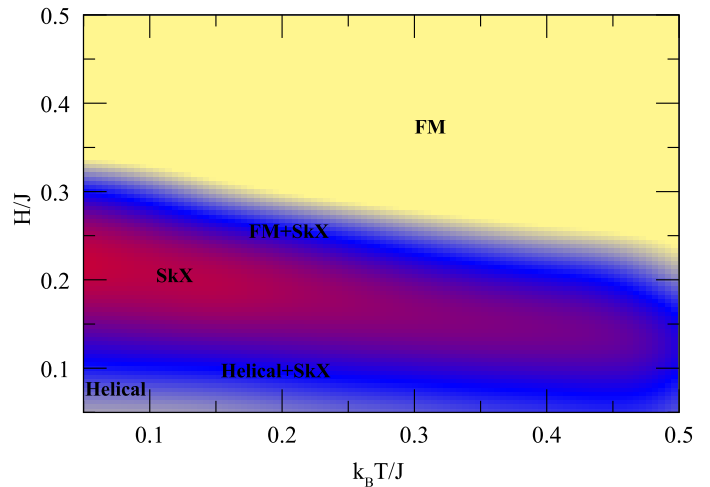


FIG. 4: The phase diagram of the model Hamiltonian.

effective field  $\mathbf{H}_{eff}$  acting on  $\mathbf{m}_{\mathbf{r}}$  is therefore given by

$$\begin{aligned}
 \mathbf{H}_{eff} &= -\partial H / \partial \mathbf{m}_{\mathbf{r}} \\
 &= J(\mathbf{m}_{\mathbf{r}+\hat{x}} + \mathbf{m}_{\mathbf{r}+\hat{y}}) + D(\mathbf{m}_{\mathbf{r}+\hat{x}} \times \hat{x} + \mathbf{m}_{\mathbf{r}+\hat{y}} \times \hat{y}) + H \hat{z}
 \end{aligned} \tag{8}$$

In the absence of external magnetic field  $H$ , a helical order is favored at low temperature. The reason is the following. As Dzyaloshinskii-Moriya interaction breaks inversion symmetry, its Fourier transformation gives a term linear in wavevector  $k$ , contrary to the  $k^2$  term contributed by the Heisenberg exchange. Energy can be minimized at a nonzero wavevector  $k \sim D/J$ , and the helical state is generated. However, the total magnetization in the helical state is zero, so that it cannot save energy from the Zeeman term. Once magnetic field is turned on, a phase transition from the helical state to the Skyrmion crystal state is observed. The large magnetic field limit corresponds to a ferromagnetic state.

In our simulations,  $D = 0.5J$ . The finite temperature phase diagram is shown in Fig. 1. It shows explicitly that the Skyrmion crystal phase is stabilized down to zero temperature. The phase transition from the Skyrmion crystal to ferromagnetic state is believed to be first order, so that dilute Skyrmions are observed at a narrow magnetic field/temperature window. In the dynamical simulations, the Skyrmion crystal corresponds to  $H = 0.15J$ , while a single Skyrmion is generated at  $H = 0.3J$ .

In the stochastic LLG equation, the choice of time step for numerical integration is an important issue. In each simulated event, the final time is set to be  $1000\hbar/J = 9.6 \times 10^{-10}$ s. The mean velocity is derived by averaging over 1000 simulated events. Fig. 2 shows the relation between average longitudinal velocity and the time step. It shows the result is convergent once the time step is smaller than 0.06ps. In the simulations in the main content, a time step of  $0.05\hbar/J = 4.8 \times 10^{-14}$ s is employed.

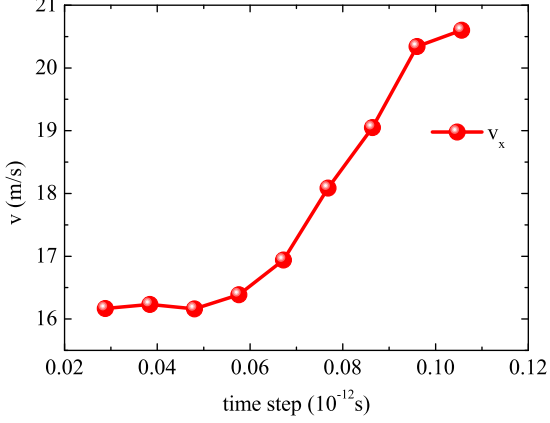


FIG. 5: The relation between the average longitudinal velocity and the time step in the numerical integration. Convergence is achieved once the time step is smaller than 0.06ps.

## II. DERIVATION OF EQ. (5)

In order to derive an equation of motion describing the effect of magnons on the equilibrium magnetization configurations, one has to separate these two degrees of freedom. To this end, let's decompose each local magnetization  $\mathbf{m}$  into slow modes  $\mathbf{m}_s$  and orthogonally fast modes  $\mathbf{m}_f$

$$\begin{aligned} \mathbf{m} &= (1 - \mathbf{m}_f^2)^{1/2} \mathbf{m}_s + \mathbf{m}_f \\ &\approx \mathbf{m}_s + \mathbf{m}_f - \frac{1}{2}(\mathbf{m}_f^2) \mathbf{m}_s + O(\mathbf{m}_f^3) \end{aligned} \quad (9)$$

where  $\mathbf{m}_s$  describes the equilibrium configuration, while  $\mathbf{m}_f$  is responsible for the magnonic dynamics. As the Hamiltonian is given by

$$H = \int d^2r \left[ \frac{1}{2} J (\nabla \mathbf{m})^2 + \frac{D}{a} \mathbf{m} \cdot (\nabla \times \mathbf{m}) - \frac{\mathbf{H}}{a^2} \cdot \mathbf{m} \right], \quad (10)$$

the effective field  $\mathbf{H}_{eff}$  in the Stochastic Landau-Lifshitz-Gilbert equation  $\dot{\mathbf{m}} = -\gamma \mathbf{m} \times (\mathbf{H}_{eff} + \mathbf{L}) + \alpha \mathbf{m} \times \dot{\mathbf{m}}$  is therefore

$$\begin{aligned} \mathbf{H}_{eff} &= -\partial H / \partial \mathbf{m} \\ &= Ja^2 \nabla^2 \mathbf{m} - 2Da \nabla \times \mathbf{m} + \mathbf{H} \\ &= Ja^2 \nabla_a [\nabla_a \mathbf{m}_s - \mathbf{m}_f (\nabla_a \mathbf{m}_f) \mathbf{m}_s - \frac{1}{2} \mathbf{m}_f^2 \nabla_a \mathbf{m}_s \\ &\quad + \nabla_a \mathbf{m}_f] - 2Da [\nabla \times \mathbf{m}_s + \nabla \times \mathbf{m}_f \\ &\quad - \mathbf{m}_f (\nabla \mathbf{m}_f) \times \mathbf{m}_s - \frac{1}{2} \mathbf{m}_f^2 \nabla \times \mathbf{m}_s] + \mathbf{H} + o(\mathbf{m}_f^3) \end{aligned} \quad (11)$$

As  $\mathbf{m}_f$  has a characteristic length scale of lattice constant  $a$ , compared to a length scale of  $(J/D)a$  for  $\mathbf{m}_s$ , it contributes larger derivatives. Therefore the leading terms of the torque are listed in the following

$$-\mathbf{m} \times \mathbf{H}_{eff} \approx -Ja^2 \mathbf{m}_s \times \nabla^2 \mathbf{m}_f - Ja^2 \mathbf{m}_f \times \nabla^2 \mathbf{m}_f$$

Here the DM terms on  $\mathbf{m}_f$  and  $\mathbf{m}_s$  can be completely neglected as only one spatial derivative will be taken into account, which is one order of magnitude smaller than the Heisenberg term. Contributions from the Zeeman term are negligible in a similar way. Besides, as  $\mathbf{m}_f$  is a fast mode behaving as a function of sine or cosine in time, by taking the average over time, linear terms in  $\mathbf{m}_f$  can be discarded as well. Therefore

$$-\mathbf{m} \times \mathbf{H}_{eff} \approx -Ja^2 \mathbf{m}_f \times \nabla^2 \mathbf{m}_f \quad (12)$$

$$= -Ja^2 \nabla (\mathbf{m}_f \times \nabla \mathbf{m}_f) \quad (13)$$

Noticing  $\mathbf{m}_f \perp \mathbf{m}_s$ , let  $\mathbf{m}_f = \mathbf{m}_s \times \mathbf{n}$ , where  $\mathbf{n}$  is an arbitrary vector perpendicular to  $\mathbf{m}_s$ . Substitute it into the expression of the torque, then

$$\begin{aligned} \mathbf{m}_f \times \nabla \mathbf{m}_f &= (\mathbf{m}_s \times \mathbf{n}) \times \nabla (\mathbf{m}_s \times \mathbf{n}) \\ &= (\mathbf{m}_s \times \mathbf{n}) \times (\nabla \mathbf{m}_s \times \mathbf{n} + \mathbf{m}_s \times \nabla \mathbf{n}) \\ &= -\mathbf{n} \nabla \mathbf{m}_s \cdot (\mathbf{m}_s \times \mathbf{n}) + \mathbf{m}_s \nabla \mathbf{n} \cdot (\mathbf{m}_s \times \mathbf{n}) \\ &\approx \mathbf{m}_s \nabla \mathbf{n} \cdot (\mathbf{m}_s \times \mathbf{n}) \\ &= \mathbf{m}_s \mathbf{j} \end{aligned} \quad (14)$$

where  $\mathbf{j} = \nabla \mathbf{n} \cdot (\mathbf{m}_s \times \mathbf{n})$  is the magnon current defined in the main content. Here again we applied the fact that  $\nabla \mathbf{n}$  is overwhelming. Consequently

$$\nabla (\mathbf{m}_f \times \nabla \mathbf{m}_f) = (\partial_\mu \mathbf{m}_s) j_\mu + \mathbf{m}_s \partial_\mu j_\mu \quad (15)$$

Assume magnon current is steady so that  $\nabla \cdot \mathbf{j} = 0$ , then the torque is given by

$$-\mathbf{m} \times \mathbf{H}_{eff} = -Ja^2 j_\mu (\partial_\mu \mathbf{m}_s) \quad (16)$$

The stochastic part of the spin transfer torque is simply

$$-\gamma \mathbf{m} \times \mathbf{L} = -\gamma (\mathbf{m}_s + \mathbf{m}_f) \times \mathbf{L} \approx -\gamma \mathbf{m}_s \times \mathbf{L} \quad (17)$$

The term  $-\gamma \mathbf{m}_f \times \mathbf{L}$  is neglected as it is a linear function of  $\mathbf{m}_f$  only, whose time average vanishes. Due to the same reason, the Gilbert damping term is

$$\alpha \mathbf{m} \times \dot{\mathbf{m}} \approx \alpha \mathbf{m}_s \times \dot{\mathbf{m}}_s + \alpha \mathbf{m}_f \times \dot{\mathbf{m}}_f \quad (18)$$

As discussed above,  $\mathbf{m}_f$  is completing cyclotron rotations with respect to  $\mathbf{m}_s$ , which is basically a sine or cosine function in time. The time derivative turns a sine function to cosine and vice versa. Therefore the time average of  $\alpha \mathbf{m}_f \times \dot{\mathbf{m}}_f$  vanishes so that

$$\alpha \mathbf{m} \times \dot{\mathbf{m}} \approx \alpha \mathbf{m}_s \times \dot{\mathbf{m}}_s \quad (19)$$

As a result, the LLG equation for  $\mathbf{m}_s$  is given by

$$\dot{\mathbf{m}}_s = -\gamma Ja^2 j_\mu \partial_\mu \mathbf{m}_s - \gamma \mathbf{m}_s \times \mathbf{L} + \alpha \mathbf{m}_s \times \dot{\mathbf{m}}_s \quad (20)$$

which is exactly the Eq. (5) in the main content.

The magnon part of this equation of motion shows similarity with the magnetization dynamics in the presence of a charge current, which is given by[1, 2]

$$\dot{\mathbf{m}}_s = \frac{\hbar \gamma}{2e} j_\mu \partial_\mu \mathbf{m}_s \quad (21)$$

here  $\mathbf{j}$  is the electric current flowing through the magnetic sample. In deriving this equation, adiabatic approximation is applied such that the spins of itinerant electrons are always parallel with the local magnetizations  $\mathbf{m}_s$ . The steady charge current contributes a term of  $H = -\frac{1}{c} \int d^2x \mathbf{j} \cdot \mathbf{a}$  to the spin Hamiltonian and leads to the equation of motion Eq. (21). Here  $\mathbf{a}_\mu = \frac{\hbar c}{2e}(1 - \cos\theta)\partial_\mu\varphi$  is the emergent gauge field associated with the magnetization configuration  $\mathbf{m}_s$ , where  $\theta$  and  $\varphi$  are the inclination and azimuthal angles of  $\mathbf{m}_s$  respectively[3]. One can easily show that the corresponding emergent magnetic field  $\mathbf{b} = \nabla \times \mathbf{a} = \frac{\hbar c}{2e} \mathbf{m}_s \cdot (\partial_x \mathbf{m}_s \times \partial_y \mathbf{m}_s)$  counts the topological charge density.

The similarity between the magnon driven magnetization dynamics and the current driven one indicates that the magnon current  $\mathbf{j}$  couples to the emergent gauge field  $\mathbf{a}$  in the same way. The reason comes from the key physical picture introduced in the main content. The magnon naturally obeys the adiabatic approximation in the leading order as the spin of a magnon is nothing but the reverse of its equilibrium direction  $\mathbf{m}_s$ . The validity of adiabaticity leads to the same structure as the current driven one. The only difference is the sign in front the  $j_\mu \partial_\mu \mathbf{m}_s$  in Eq. (20) and Eq. (21). This is because the magnetization  $\mathbf{m}_s$  is parallel with the spin of itinerant electron, while anti-parallel with the spin of magnon.

- 
- [1] Ya.B. Bazaliy, B.A. Jones, and S. C. Zhang, Phys. Rev. B **57**, R3213 (1998).  
 [2] G. Tatara, H. Kohno, and J. Shibata, Phys. Rep. **468**, 213 (2008).

- [3] J. Zang, M. Mostovoy, J. H. Han, and N. Nagaosa, Phys. Rev. Lett. **107**, 136804 (2011)